Supporting Information

DESIGNED-BY-PURPOSE POWER SOURCES: A CARDBOARD PRIMARY BATTERY FOR SMART PACKAGING

*Marina Navarro-Segarra**[a,b] *Omar A. Ibrahim,*[c] *Iñigo Martin-Fernandez,* [b] *Carles Tortosa,* [b,c] *Joseba M. Ormaetxea,*[b] *Manuel Bauman,*[d] *Marcel Weil* [d,e] *and Juan Pablo Esquivel* *[a,b,f]

[a] BCMaterials, Basque Centre for Materials, Applications and Nanostructures, UPV/EHU Science Park, 48940 Leioa, Spain

[b] Instituto de Microelectrónica de Barcelona, IMB-CNM (CSIC), C/dels Til·lers s/n, Campus UAB, 08193 Bellaterra Barcelona, Spain

[c] Fuelium S.L., Edifici Eureka, Av. Can Domènech S/N, 08193 Bellaterra, Barcelona Spain

[d] ITAS, Institute of Technology Assessment and Systems Analysis, KIT – Karlsruhe Institute for Technology, Karlsruhe, Germany

[e] HIU, Helmholtz Institute Ulm for Electrochemical Energy Storage, Ulm, Germany

[f] IKERBASQUE, Basque Foundation for Science, 48009 Bilbao, Spain

Contents

Scenarios for battery-powered IoT devices in smart packaging

After the evaluation of the current scenarios of battery usage in smart packaging applications, some of the most typical have been identified as:

A: Conventional portable primary power sources (i.e., coin cell or alkaline batteries) are applied to smart packaging solutions that, after the use phase, are detached from the package and repurposed for a second-life application. This scenario relies on end-consumer responsibility.

B: Conventional portable primary power sources (i.e., coin cell or alkaline batteries) are applied to smart packaging solutions that, after the use phase, are detached from the package and recycled as battery waste. This scenario requires end-user responsibility, efficient battery waste collection routes and sustainable recycling procedures and facilities. The use of standard battery formats still faces challenges such as the lack of adaptability and the high environmental footprint associated with the extraction, processing, storage, and transport of all unused materials contained in the battery.

C: Conventional primary portable power sources (i.e., coin cell or alkaline batteries) are applied to smart packaging solutions that, after the use phase, are thrown away together with the cardboard box disturbing the paper recycling processes. It should also be taken into account that the cardboard and paper waste stream has the highest recycling rate among all materials, reaching almost 74% in 2020 within the EU.[1] Furthermore, cardboard packaging materials have a highly circular life cycle, as their fibers may be recycled up to 25 times.[2] Hence, this scenario has a significant impact on a well-stablished and robust recycling flow.

The present approach takes scenario C as the framework to develop a battery designed-by-purpose in an ecologically benign way.

Battery demonstrator-associated materials and energy consumption

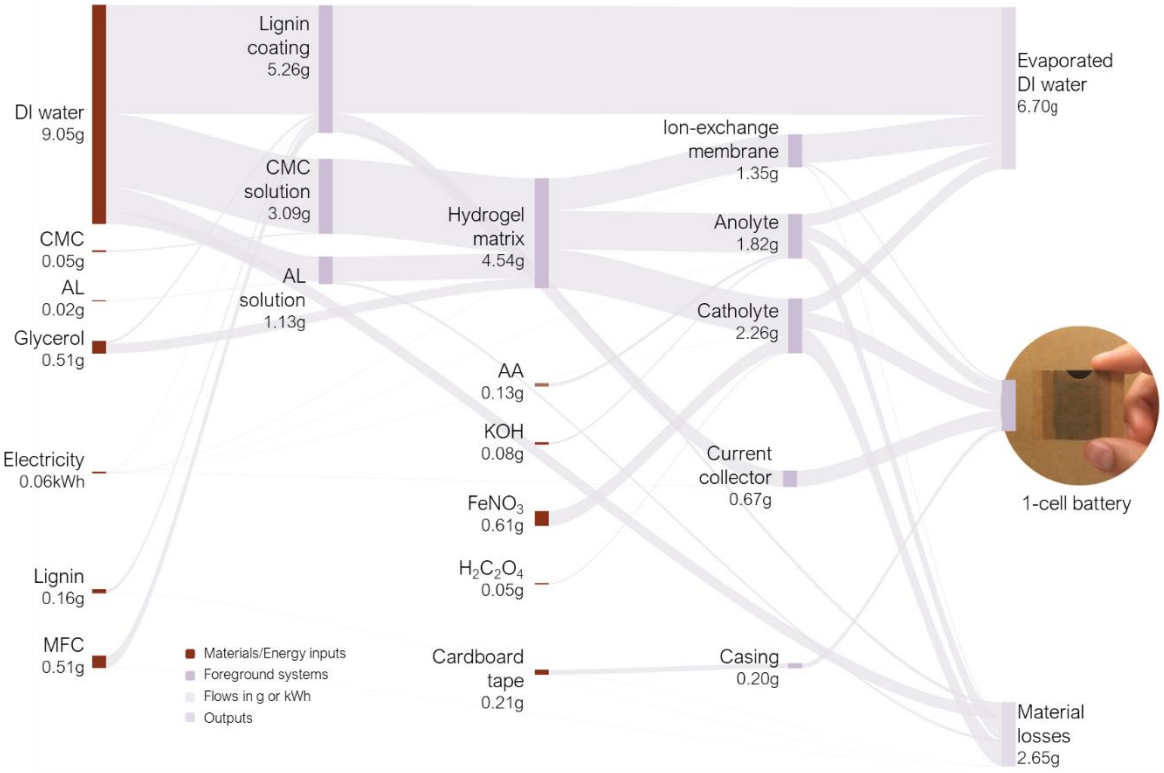

Figure S1. Visual Life Cycle Inventory for 1-cell battery prototype.

Figure S1 is a representation of the flows of materials quantities inputs (g), energy inputs (kWh) and outputs (i.e. evaporated deionized (DI) water and material losses) to create 1-cell battery prototype. The quantities correspond to the laboratory scale fabrication protocol for a 20 prototypes batch then allocated for one battery. The energy required for stirring, laser engraving and membranes drying have been directly measured with a plug-in power meter. The provided data can serve as a first step to carry out a prospective life cycle assessment

Packaging industry and adhesive label fabrication methods at industrial scale

Packaging is a highly automatized industry in a state of constant evolution. It covers from the creation of securing material (such as bubble wrap) to the aesthetics involved during the items' display. Like other industries, packing is not immune to global trends; in fact, in recent years the blooming of e-commerce alongside the spread of sustainability concerns among consumers, has driven the packing market to seek more efficient logistics and more sustainable technology innovation. This is how, in the last years, concepts such as smart packaging and the internet of packaging have arisen and fostered the adoption of smart and sustainable solutions promoting a more consumer-, brand- and environmentally friendly product packaging. Regarding the packaging production industry, it is mainly based on roll-to-roll manufacturing methods. Hereinafter is explained in more detail the packaging production system for adhesive labels, since these fabrication processes have served as inspiration to develop the prototype presented in this work.

Most adhesive labels, or stickers, are made of vinyl films. Those that are made from polyvinylchloride (PVC) polymer are typically manufactured in two ways: by calendering and by casting. Calendered vinyl is cheaper than cast vinyl and serves many applications. Cast vinyl is a premium grade vinyl made with high-quality plasticizers and is much thinner and stretchier than calendered vinyl.[3–5] In this case scenario, the cast vinyl process is the closest to the hydrogel membranes prepared along the work of this article, which are also prepared by casting. Thus, it will be the only manufacturing method analysed. Cast vinyl is made by preparing a liquid mixture of different components: PVC resin, pigment, plasticizer, UV-absorber, fillers and heat stabilizers. Later, a thin film of this mixture is poured on a casting sheet, which sets its texture and allows its mobility through the process. Immediately after, the cast film goes through an oven where all components are cured, and solvents evaporate. The film hardens and finally is wound up in large rolls.[3–5] Figure S2a shows a diagram of this process, which could be adapted to large-scale manufacture of the hydrogel membranes synthesized in this work, since they are also prepared by casting - but using deionized water as solvent, which lessens the environmental impact and monetary cost.

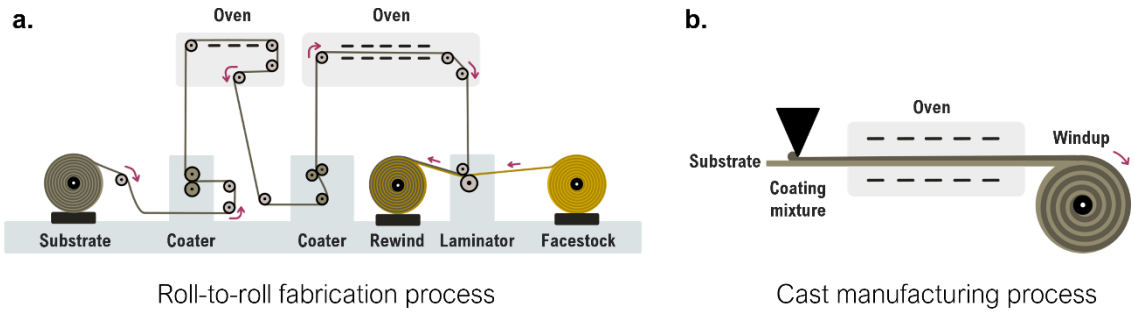

Figure S2. Diagrams for adhesive labels' industrial manufacturing: **a.** Sheet lamination process in roll-to-roll large scale manufacture. **b.** Cast vinyl: coating, curing and windup.

Subsequently, a layer of adhesive is coated on the less absorbent substrate web, by means of different techniques such as: wire rod, knife-over-roll, reverse-roll, gravure, extrusion die, slot die, curtain…[6] Usually this substrate is the liner, a thin sheet made of silicone-coated paper or, less often, polyethylene terephthalate (PET) polymer, which protects the adhesive and gets easily released.[7] Finally, a process called sheet lamination is used to stack the adhesive and the facestock layers. It is a process in which two or more flexible packaging webs are joined together using a bonding agent.[8,9] It is better suited for simple shapes, paper-based or polymeric materials and embedded electronic devices. Figure S2b shows a schematic diagram of this process. The lamination process is key for assembling packaging multilayer composites, and in the case scenario of this work, this method can be used on large scale manufacture for assembling the different membranes of the battery (anodic, ionic and cathodic; presented in the main text).

Patterning and characterization of Laser-Induced Graphene

Laser-induced graphene (LIG) is a graphitic porous material that has been reported to have a high surface area and remarkable chemical, physical and electronic conductivity of graphene. LIG forms upon photochemical and photothermal processes occurring when lasing some precursor composed of C-C bonds. Briefly, the CO_2 laser outputs a 10.6 μm centered band, which is absorbed by those C−C bonds, creating localized high temperature and pressure, breaking C-O, C=O and N-C bonds. Then, carbon atoms rearrange to form 3D porous graphene (Figure S3a). Until the discovery of LIG, the most widely used fabrication techniques were chemical vapour deposition and hydrothermal processing. These require either high-temperature steps, long synthesis routes or high economic costs. Graphene patterning by hydrated graphene oxide (GO) laser writing is possible, but it is unappealing as GO is expensive and involves lots of acidic and oxidizing waste. All in all, LIG technique stands out as a simpler, lower energy, zero waste and easier implementable choice against its direct competition to produce 3D porous graphene.

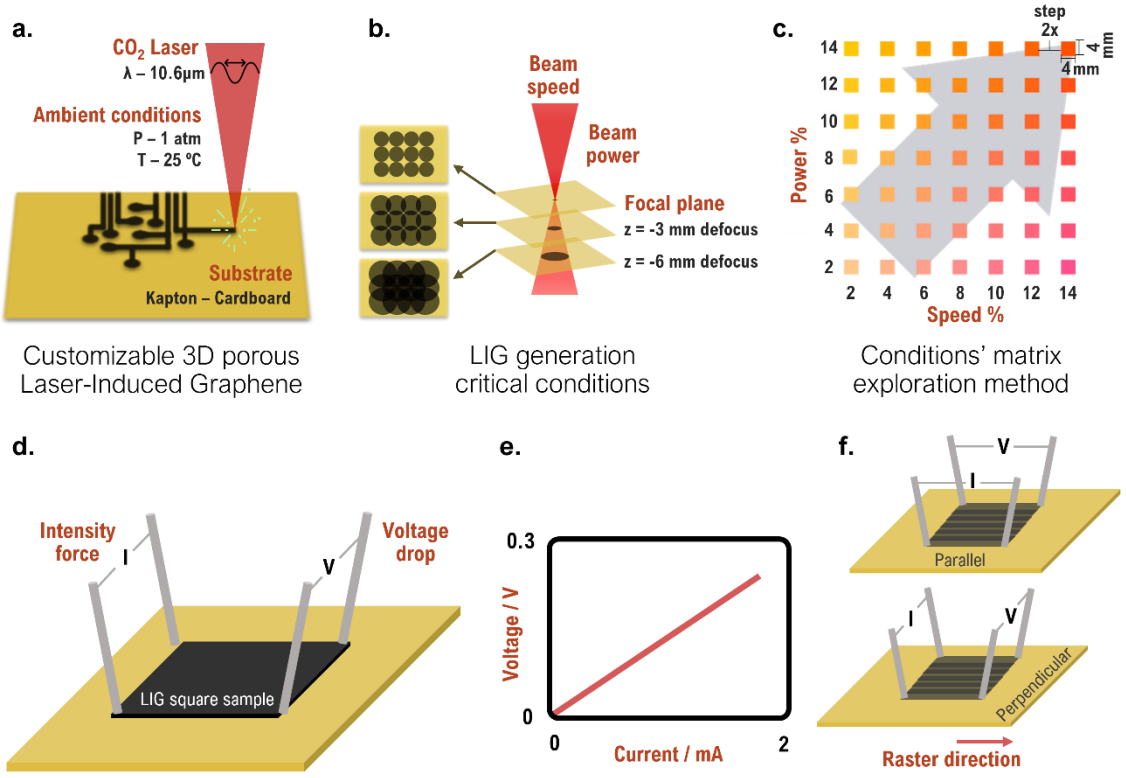

Figure S3: a. Laser-Induced Graphene (LIG) technique allows a patterned graphene generation in a single step using a CO_2 laser and at ambient conditions. **b.** The beam's speed over the substrate, its power, and its focal plane engravement were the studied process' parameters, **c.** through the matrix exploration method, as lasing conditions critically influence LIG's successful generation. **d.** The electrical resistance has been evaluated using the Van der Pauw technique in a four-vertice station. **e.** The sheet resistance is obtained through the analysis of the I-V diagram, in this work. **f.** This analysis was performed in two orientations (parallel and perpendicular to the raster direction) to evaluate LIG's anisotropy.

Very fine control of both the precursor substrate and the lasing conditions is needed to obtain LIG with controlled quality and uniformity. Figure S3c is a 7x7 matrix combining a lasing power percentage (P) with a lasing speed percentage (S), to optimize LIG generation conditions and

export the technique to the precursor substrates of interest. The laser was always defocused 3 mm (Figure S3b). After the window of the laser conditions for LIG creation was defined, the resistance of the produced materials was assessed by the Van der Pauw method to assess the quality of the LIG (Figure S3d to S3f) using Equation (S1). These measurements showed anisotropy, which is assigned to the raster-based patterning of LIG (SI-S4 and SI-S5).

Regarding the substrate, later studies have shown that PI is not the only possible precursor for LIG. Laser-induced graphene has been produced on many other organic substrates so far. Biobased precursors include cellulose nanofiber, wood and lignin. J. M. Tour et al. tested cork, coconut, potato skin, bread, cotton paper, cardboard and cloth. Several plastic polymers (like Kevlar, PEI or PSU) have also been used with success. Altogether, the resulting LIG has shown dependence on the precursor material. For example, in lignocellulosic biomaterials, a higher lignin content over cellulose and hemicellulose generates fewer defects on the obtained graphene. This can be related to the specific carbon content of each precursor material: lignin is a macromolecule with 63-66% C content, while cellulose and hemicellulose have about 44% C content.[10–12] In comparison, PI tape has a 69% of C content.[13] This is not the only factor influencing LIG quality since, as mentioned above, CO_2 commercial laser outputs a specific centered band and thus breaks only specific bonds. As a consequence, LIG's resulting quality will highly depend on the molecular structure bonds' nature of the precursor material beyond its elemental composition: PI has prominently C-C, C=C, C-N, C-O and C=O links;[13] whereas lignin has primarily C-C, C=C, C-O-C, -OH, C=O, COOH and -OCH_3.[14] Due to lignin's high chemical variety and multiplicity of structures, C release, i.e., atomic linkage breaking, will be less homogeneous than, for example, PI tape, which has a much more homogeneous structure and composition.

Laser conditions' screening for electrically conductive LIG

Matrix screening of laser conditions (Speed-Power) was performed on three different cardboard pre-treated precursors and, after iteratively adapting and narrowing lasing conditions, the S-P ranges which lead to the most promising LIG were (for all the precursors): Speed, from 7% to 13%; and Power, from 10 to 12% (percentage refers to laser's maximum possible output). All substrates were engraved with 3-mm defocus**.** Figure S4 illustrates the sheet resistance values of the LIG resulting from the S-P combinations.

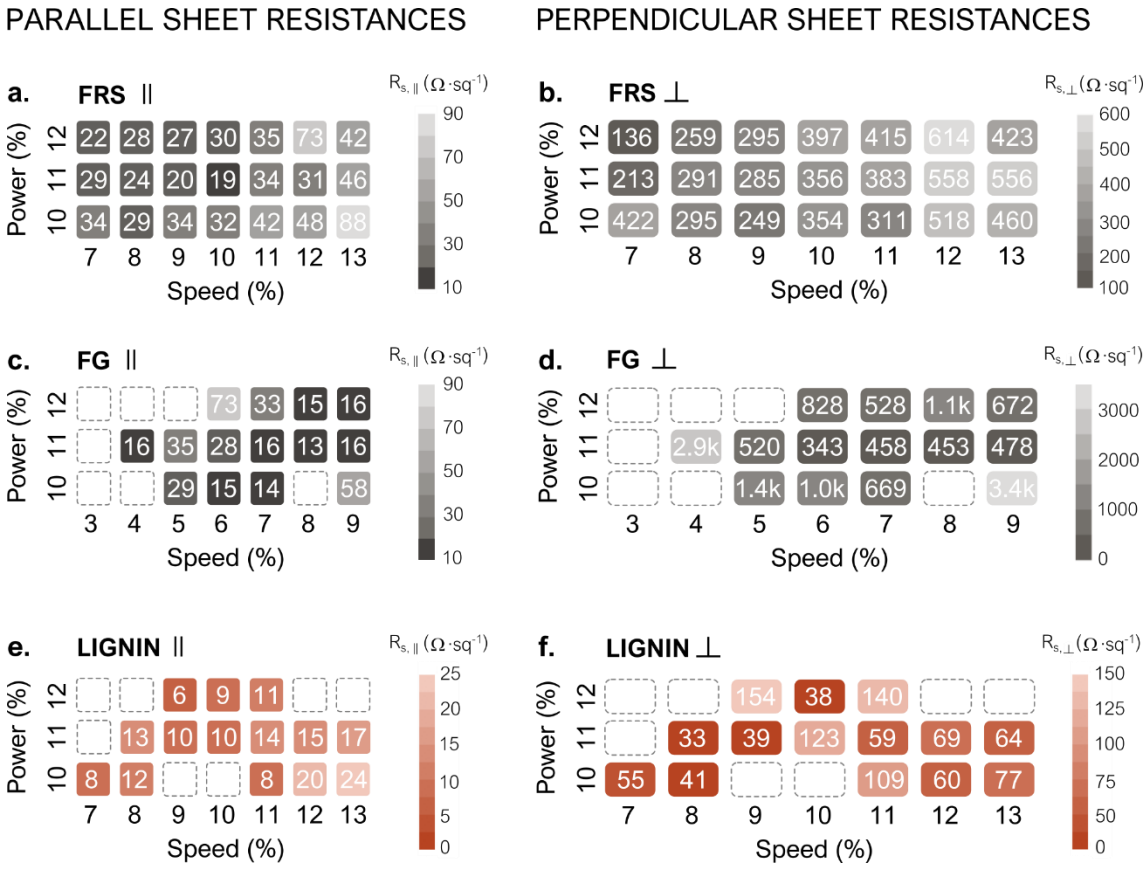

Figure S4. Sheet resistance values of LIG were obtained on the three cardboard coatings (**a,b** - FRS; **c,d** – FG; **e,f** – LIGNIN) within a range of laser conditions (Speed-Power). Parallel and perpendicular refer to the relative orientation between Van der Pauw measurements concerning the laser engraving directions. White spaces denote S-P conditions where LIG did not form, thus being non-conductive and marking the boundary conditions for LIG's formation.

LIG's morphology comparison on cardboard pre-treated with Fire Guard or Fire-Retardant Spray

The two flame retardants studied in this work as cardboard pre-treatment led LIG with similar sheet resistance characteristics, i.e., Rs, || ~ 50Ω/sq. However, as can be observed in Figure S5, while with Fire Guard an uncertain boundary definition was found, when using Fire Retardant Spray the shape transference from the CAD design to the laser patterned was trustworthy.

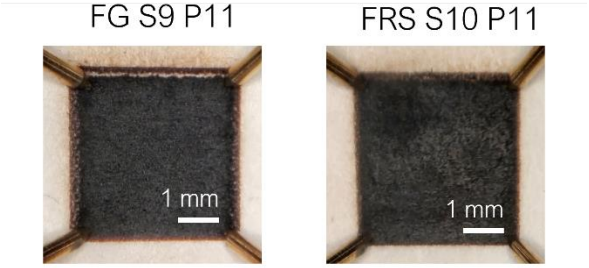

Figure S5: Border definition comparison on LIG squares engraved over cardboard with Fire Guard (FG) or Fire Retardant Spray (FRS) as pre-treatments. Square 4x4mm size.

Anisotropic nature of LIG

Figure S6 shows SEM images of the surface of LIG formed on polyimide, lignin and FRS-coated cardboard. The generated LIG shows a topography that matches the direction and step of the laser engraving, where patterned lines can be observed. This phenomenon arises as the explanation for the directional dependence of LIG's sheet resistance.

Figure S6: SEM images of LIG surface engraved over the polyimide, lignin coating over cardboard and Flame Retardant Spray (FRS) over cardboard. Scale bar: 100 µm.

Raman spectra for PI, LIGNIN and FRS substrates before lasing

Figure S7 shows the Raman spectra from the different substrates used to generate LIG before lasing them. No remarkable peaks are observed. The strong backgrounds relate to the fluorescence of the materials caused by the laser wavelength (532 nm). [15]

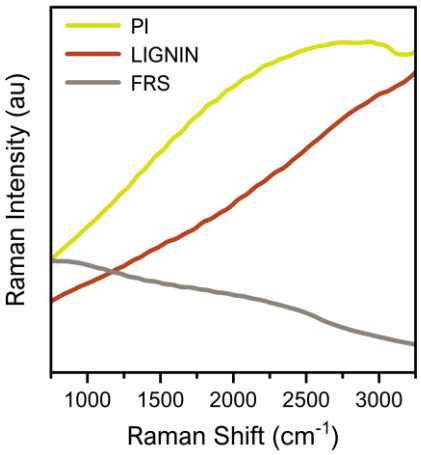

Figure S7: Representative Raman spectra from the polyimide substrates (PI) and from the cardboard substrates treated with the lignin coating (LIGNIN) or with the flame-retardant spray (FRS) before lasing them.

Battery single-cell and 4-stack cell prototype components

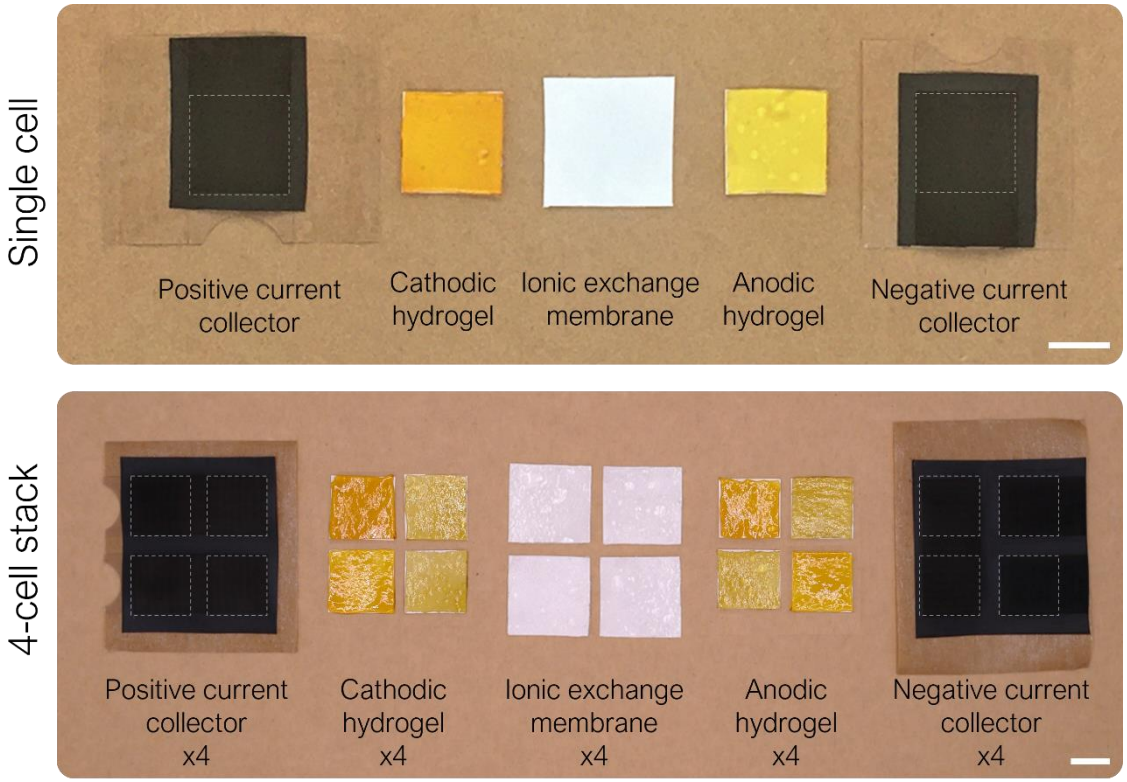

Figure S8. Exploded view of the battery single cell and 4-stack cell prototypes. The label-like prototypes are based on a layered design: the central part is composed of self-standing hydrogel layers that act as a separator, anode, and cathode; then, LIG current collectors are engraved on a lignin-based membrane and attached to a recyclable cardboard-tape, which acts both as casing and backing material. For the sake of clarity, a white backing card has been used in these photographs to enhance the hydrogel layers' visual contrast; and grey dotted lines highlight the hydrogel layer placement on the LIG current collectors. Scale bars: 1 cm.

Materials and methods

Chemicals: microfibrillated cellulose (MFC**)** Exilva P 01-V was provided by Borregaard (Sarpsborg, Sarpsborg). All following chemicals were purchased from Sigma Aldrich (Sigma Aldrich, St Louis, Missouri, USA): lignin alkali (ref: 471003), glycerol (ref: G7757), sodium alginate (ref: W201502), iron (III) nitrate nonahydrate (ref: 221473), ascorbic acid (ref: A4403), oxalic acid (ref: O0376), potassium hydroxide (ref: 221473) and potassium hexacyanoferrate(III) (ref: 244023). While carboxymethylcellulose sodium salt was purchased from Glentham Life Sciences (ref: GC7698, Glentham Life Sciences Ltd, Corsham, United Kindom).

All solutions were prepared in deionized water.

Coatings preparation and application: Manilla cardboard from recycled office folders was used as substrate. Phosphate ammonium ForcedField FireGuard for Fabrics (Shield Industries, Georgia, USA) and boric acid-based Flame Retardant Spray (FireChief, Oakham, UK) were purchased online and used as received from their spray bottles. Each product was separately applied to a 10x10 cm^2 cardboard square by spraying 6 times and dried overnight at room temperature. Lignin coating preparation was based on a 1% w/v MFC dispersion. 10% w/v MFC (2 g) was dispersed in deionized water (18 mL) using a T 25 digital ULTRA-TURRAX (IKA-Werke, Staufen, Germany) dispersion instrument, following manufacturer instructions, i.e., 10000 rpm for 5 minutes. Then, pure lignin alkali (0.6 g) was also added and dispersed. Finally, 0.32 mL of glycerol was added as plasticizer. To create the coating, 20 mL of dispersion was poured over the cardboard using an 8.6 cm diameter petri dish as a container and dried for 72 hours in an incubator at 25 ºC (ET 618-4, 135L, Lovibond®). To use the coating as self-standing membranes, 40 mL of dispersion were poured over a petri dish (8.6 cm diameter)

Hydrogel matrix and redox gels preparation: A dilution of sodium alginate (AL) at 2% w/v concentration was prepared in deionized water (DI) by magnetically stirring at 80 ºC for 30 minutes. Simultaneously, carboxymethyl cellulose (CMC) 1.5% w/v was prepared (also in DI water) by stirring at room temperature for 12 hours. Then, the hydrogel matrix was prepared by mixing both dilutions at 75CMC:25AL proportion and doping with a 5% w/v of glycerol. The mixture was then homogenized over 2 hours by magnetic stirring. Later, to create the separator, the obtained hydrogel matrix (15 mL) was poured into an 8.6 cm diameter petri dish and dried at 25 ºC for 12 h in a forced flow-air oven (Digitronic-TFT model, J.P. Selecta, Barcelona, Spain). Similarly, the anodic matrix was synthesized by incorporating ascorbic acid (0.5 M) and KOH (1 M) into the hydrogel matrix. Respectively, the cathodic matrix was synthesized by adding $Fe(NO_3)_3$ (1 M) and oxalic acid (0.25 M). The obtained blends (5.8 mL) were poured in a 5.4 cm diameter petri dish. The redox membranes were dried in the forced flow-air oven until 39.2 % humidity stabilized for the cathode and 6.3 % for the anode.

Lasing process: Patterns were designed using Inkscape (open-source vector graphics editor) and then sent to the lasing system. The laser-induced materials' study, presented in this work, has been performed with an Epilog Legend Mini 24 CO_2 laser engraver (Golden, USA). The laser has two modes of operation, engrave or cut. In this work, engrave mode was used to generate the LIG samples. 1200 DPI resolution and autofocus modes were pre-selected for all the generated samples. While the speed of the moving lens (S) and power (P) are chosen from 1% to 100% of the designed value according to the predesigned condition matrix. Being 30W the maximum theoretical power reached by the laser (i.e. P = 100%) in the case of this particular laser. It is worth mentioning that over the course of this work, the laser maximum power was measured with a Pronto 205 detector from Gentec-EO, registering a maximum power of ~20.5 W. A specific conditions matrix was optimized for each cardboard treatment.

Electrical characterization of LIG: The LIG material was electrically characterized in a four-point probe station (EP6, Suss Microtec). The Van der Pauw method was used to determine the sheet resistance (R_s) and applied as a screening methodology. Figure S3, schematically describes the basis of this technique. Briefly, the four vertices of a sample are electrically contacted with four metallic needles, then a current scan is forced between two vertices while the voltage drop between the opposite two is recorded. Current was swept from 0 to 2 mA with a 4 µA step. From the I-V curve's slope, in the parallel or perpendicular orientation, an average sheet resistance value of the samples (according to that orientation – $R_{s,\parallel}$ and $R_{s,\perp}$, respectively) was calculated by applying Equation (S1).

$$R_s = \frac{Ln\ 2}{\pi \cdot V} I \qquad (S1)$$

Being, I and V the applied current and voltage respectively, and $\frac{Ln\ 2}{\pi}$ the geometrical correction factor, where the final resistivity was later calculated by multiplying the sheet resistance value by the SEM measured thickness of the LIG for each precursor.

Morphological assessment: The LIG samples yielding the highest electrical conductivity was further studied using a Scanning Electron Microscope (SEM, Carl Zeiss Auriga model). 1kV electron acceleration was selected for surface and cross-section imaging. In order to take cross-section pictures, the samples were cut with a scalpel. A stage with metal tweezers was employed to limit the drift issues at higher magnification analysis (15Kx).

Raman spectroscopy of the samples was completed in a Horiba Xplora Plus confocal Raman microscope equipped with a 532 nm laser and x10 and x50LD objectives. The spectra of each of the sample types in the main text was calculated out of 27 spectra (3 distributed maps, each composed of 9 single spectra).

Electrochemical measurements: All the electrochemical measurements were performed using a PalmSens4 potentiostat/galvanostat/impedance analyser (Palmsense BV, Houten, The Netherlands).

LIG electrodes' electrochemical characterization was performed by cyclic voltammetry analysis adapting the voltage window and with a 20 $mV \cdot s^{-1}$ scan rate for all samples. A conventional three-electrodes electrochemical cell was assembled using a commercial Ag/AgCl (3 M, KCl) and a platinum counter electrode (CH Instruments Inc., TX, USA). Ferricyanide (0.1 M) was selected as well-known electroactive species and phosphate-buffered saline (1M, KCl) was used as aqueous electrolyte. The Electrochemical Active Surface Area (ECSA) was calculated from current peaks using Randles–Ševčík[16,17] equation for reversible (Eq. S2), and (Eq. S3) for quasi-reversible systems.

$$i_p = 0.446nFAc^0\left(\frac{nFvD}{RT}\right)^{\frac{1}{2}} \qquad (S2)$$

$$i_p^{qr} = \pm(2.65 \cdot 10^5)n^{\frac{3}{2}}ACD^{\frac{1}{2}}v^{\frac{1}{2}} \qquad (S3)$$

Where, n is the number of electrons transferred, F is the Faraday constant, A is the area of the electrode, C_0 is the analyte bulk's concentration, ν is the scan rate, D is the diffusion coefficient, R is the gas constant and T is the temperature. The electron transfer rate constant (k^0) was computed via the Nicholson method.[18]

Hydrogel membranes' ionic conductivity was evaluated by Electrochemical Impedance Spectroscopy (EIS) analysis from 1 kHz to 1 MHz. Then, the value of the hydrogel matrix's conductivity (σ) was obtained from the following expression (Eq. S4):

$$\sigma = \frac{d}{RA} \qquad (S4)$$

Where, d is de distance between electrodes (equivalent to the membrane's thickness in this case), A is the electrode's contact area and R is the ion mobility resistance of the sample, which is obtained from the total impedance when the imaginary component is zero.

Redox species' electrochemical behavior was assessed also in the three-electrode cell using a glassy carbon electrode (0.071 cm^2) as working electrode (CH Instruments Inc., TX, USA).

Battery polarization and power curves were generated using linear sweep voltammetry technique, sweeping from pre-recorded OCV values to 0V at a scan rate of 20 $mV \cdot s^{-1}$, in all cases. Discharge curves were recorded under different demanded currents by chronopotentiometry technique. All tests were performed at room temperature.

Battery demonstrators and final prototypes fabrication: The devices' current collectors were designed using Inkscape and engraved using the CO_2 laser (Epilog Legend Mini 24 instrument) on top of the desired precursor substrate. The membranes were prepared as described above and then they were manually cut using a pattern into the desired dimensions (15 x 15 mm in the case of the redox gelified hydrogels and 20 mm x 20 mm for the ion-exchange membrane). Most of the demonstrators' assembly was done layer by layer using an alignment pattern.

For the final recyclable battery prototypes, the current collectors were engraved on a self-standing lignin membrane and commercial adhesive tape was used as the battery substrate and casing. The tape (KRAFT 700) was provided by the company UBIS (Hernani, Basque Country, Spain), which has been certified as recyclable (AENOR RP E19.01 (2020-11)). The material also holds the Forest Stewardship Council (FSC®) C157528 certification.

End-of-life assessment:

The 4-cell stack prototype attached to the cardboard box and to the envelope (KAC006 and KSK100, from Kartox, Barcelona, Spain) has been defined as recyclable according to the recyclability technical definition on UNE-EN 13430 Packaging - Requirements for packaging recoverable by material recycling norm and its annexes (CR16688).

The experimental evaluation of the recyclable nature of the prototype was carried out by ITENE technology center by applying the ATICELCA 501/19 standardized methodology in compliance with the norm UNI 11743:2019 Paper and board - determination of parameters of recyclability of cellulose-based materials and products.

Supplementary References

1 EPRC, *Monitoring Report 2020. European Declaration on Paper Recycling 2016-2020*, 2021.

2 Packaging Europe, Paper and cardboard recycling reach record high across Europe, https://packagingeurope.com/paper-and-cardboard-recycling-have-reached-record-high-acros/, (accessed 31 May 2021).

3 A. Emanuel Ximim Gavim, R. de Oliveira Mascarenhas, L. Selzler Sbrissia, J. Valter Barbosas Júnior, T. Reges Casagrande and A. Gerniski Macedo, *Mater Lett*, 2023, **338**, 134065.

4 What is sticker printing and How it works? - Shockwave Print, https://shockwaveprint.com/what-is-sticker-printing/, (accessed 30 November 2023).

5 Difference Between Cast and Calendered Vinyl | S&F Supplies News & Updates, https://sfsupplies.com/news/difference-between-cast-and-calendered-vinyl/?__cf_chl_tk=C9ahUGw68_LfWjmiofj_EZqbPexVHnKCVfoD_q2mdTk-1685632369-0-gaNycGzNGpA, (accessed 30 November 2023).

6 Thermoforming of Single and Multilayer Laminates: Plastic Films Technologies ... - Syed Ali Ashter - Google Books, https://books.google.es/books?hl=en&lr=&id=nUEnAAAAQBAJ&oi=fnd&pg=PP1&dq=10.1016/B978-1-4557-3172-5.00004-9&ots=xFN_PqUTja&sig=QImxdgVw6ApGrdA49e5vOEjukBM#v=onepage&q=10.1016%2FB978-1-4557-3172-5.00004-9&f=false, (accessed 30 November 2023).

7 Biodegradable Paper Stickers: All You Need to Know | Sticker it, https://stickerit.co/en-eu/blogs/general/biodegradable-paper-stickers-all-you-need-to-know, (accessed 30 November 2023).

8 Manufacturing Pressure-Sensitive Adhesive Products: A Coating and Laminating Process | 2005-04-01 | Adhesives & Sealants Industry, https://www.adhesivesmag.com/articles/86079-manufacturing-pressure-sensitive-adhesive-products-a-coating-and-laminating-process, (accessed 30 November 2023).

9 Y. Y. C. Choong, *Digital Manufacturing: The Industrialization of 'Art to Part' 3D Additive Printing*, 2022, 145–182.

10 S. Ma, F. He, D. Tian, D. Zou, Z. Yan, Y. Yang, T. Zhou, K. Huang, H. Shen and J. Fang, *Biogeosciences*, 2018, **15**, 693–702.

11 E. Adler, *Wood Sci Technol*, 1977, **11**, 169–218.

12 Lignin, organosolv | C81H92O28 | CID 73555271 - PubChem, https://pubchem.ncbi.nlm.nih.gov/compound/Lignin_-organosolv, (accessed 30 November 2023).

13 V. N. Rai, B. Jain, C. Mukherjee, P. Choudhary, P. Saxena and A. Mishra, *Radiation Effects and Defects in Solids*, 2020, **175**, 879–891.

14 C. W. Lahive, P. C. J. Kamer, C. S. Lancefield and P. J. Deuss, *ChemSusChem*, 2020, **13**, 4238–4265.

15 O. G. Rehrauer, B. R. Mankani, G. T. Buzzard, B. J. Lucier, D. Ben-Amotz, J. E. Vornehm, A. J. Dong, R. W. Boyd, Z. Shi, D. S. Wilcox, G. T. Buzzard, B. J. Lucier, P. Wang, D. Ben, J. Zhao, H. Lui, D. I. McLean and H. Zeng, *Optics Express, Vol. 23, Issue 18, pp. 23935-23951*, 2015, **23**, 23935–23951.

16 L. Kolthoff and N. Y. Polurogruphy (interscience, *Transactions of the Faraday Society*, 1948, **44**, 327–338.

17 A. Ševčík, *Chempluschem*, 1948, **13**, 349–377.

18 R. S. Nicholson, *Anal Chem*, 1965, **37**, 1351–1355.